ISSN: 0128-7680
Pertanika J. Sci. & Technol. **17 (2)**: 245 – 262 (2009)

Target Detection in Forward Scattering Radar

Mohamed Khalaf alla Hassan Mohamed,
Raja Syamsul Azmir Raja Abdullah* and M.F.A. Rasid
Microwave, Millimetre Wave and Radar System Laboratory,
Department of Computer and Communication Systems, Faculty of Engineering,
Universiti Putra Malaysia, 43400 UPM, Serdang, Selangor, Malaysia
**E-mail: rsa@eng.upm.edu.my*

ABSTRACT

This paper analyses electromagnetic signal scattered from the target crossing the Forward Scattering Radar (FSR) system baseline. The aim of the analysis was to extract the Doppler signal of a target under the influence of high ground clutter and noise interference. The extraction was used for the automatic target detection (ATD) in the FSR system. Two extraction methods, namely Hilbert Transform and Wavelet Technique, were analyzed. The detection using the Hilbert Transform is only applicable for some conditions; however, the detection using the Wavelet Technique is more robust to any clutter and noise level. From 55 sets of signal, only 4% of false alarm was detected or occurred when the Wavelet Technique was applied as a detection scheme. Two sets of field experimentation were carried out and the target's signal under the influence of high clutter had successfully been detected using the proposed method.

Keywords: Forward Scattering Radar, Hilbert Transform, Wavelet Denoise, target detection

ABBREVIATIONS

FSR: Forward scattering radar
FSCS: Forward scattering cross-section
RCS: Radar cross section

INTRODUCTION

Forward scattering radar (FSR) is an operational mode of bistatic radar which corresponds to the case when the bistatic angle is nearly 180°. The FSR offers a number of peculiarities which make it a viable interest. Its most attractive feature is the steep rise in the target radar cross section (RCS) as compared to the traditional monostatic radar (Glaser, 1985; Stimson, 1983; Jackson, 1986), and this particular feature improves the sensitivity of the radar system. The forward scattering RCS mainly depends on the target's physical cross section and the wavelength, and at the same time, it is independent on the surface shape of target and any radar absorbing material (RAM) coating which reduces the RCS of the target in the traditional radar (Boyle, 1994). This feature has made the FSR robust to stealth technology. In addition, the FSR only requires a relatively simple hardware and has a long coherent interval of the received signal. Moreover, the FSR receiver can utilise radiation from non-cooperative transmitter, without revealing its location. In a hostile environment, this is

Received: 21 January 2008
Accepted: 16 July 2008
*Corresponding Author

highly desirable as the receiver may be used covertly. All these advantageous features create a 'come back' interest to the FSR after it was abandoned since World War II (Willis, 1995). As far as the authors' knowledge is concerned, only a few researchers and research labs are seriously working in this area (e.g. Abdullah *et al*., 2004; Blackman, *et al*., 2000; Cherniakov *et al*., 2006).

The basics of the FSR can be found in the works of Willis (1995) and Chernyak (1998), whereas research on target detection, coordinate estimation and automatic classification can be found in Abdullah *et al*. (2004), Raja Abdullah *et al*. (2005) and Cherniakov *et al*., 2006). Despite the results reported in the stated literature, most studies carried out on the FSR have only been carried out in a small number of scenarios and most publications dedicated to the FSR studied on airborne. The more recent studies, which focused on ground application (Abdullah *et al*., 2004; Cherniakov *et al*., 2006), did not assume any denoising process of different noise levels masking the received signal in which it made the detection process more difficult.

This paper concentrates on the method of extracting signal scattered from the ground target crossing the FSR baseline. Typical ground vehicle (car) has been used as a target. The signal scattered from the target is embedded and hidden inside the high clutter and noise interferences. Two methods, namely the Hilbert Transform and Wavelet with the capability of denosing, were analyzed to predict the existence of a target. Using these techniques has been shown to effectively predict target crossing the FSR baseline. To the best knowledge of the authors, this paper is amongst the earliest documented discussion dedicated to ground clutter rejection in the FSR. Thus, using FSR for detection and classification of ground targets, together with its low cost system, various applications in civil, defense, medical and security systems could be found.

FORWARD SCATTERING RADAR BASIC AND THEORY

This section summarizes the basic technical aspects in the FSR and more details can be found in Abdullah *et al*. (2004) and Cherniakov *et al*. (2006). As discussed in the earlier section, the FSR introduces a specific case of a more general class of radar, namely the bistatic radar (BR). The key peculiarity of the FSRs is that, in contrast to their monostatic and bistatic counterparts, they exploit an effect of electromagnetic wave shadowing a target, rather than scattering from the target. This fact puts an essential restriction on the FSR topology, since the target shadow exists within a relatively narrow corridor of $<20^{o}$ around the baseline, that is, the line connecting the transmitter and the receiver. Another consequence is that the system loses its range resolution. The FSR system, as shown in *Fig. 1*, comprises of a transmitter (*Tr*) with *fc* central frequency and an appropriate wavelength (λ), and of a receiver (*Re*) separated by a distance (*b*) from the transmitter. The target (*Ta*) is assumed to be moving along a trajectory which crosses the baseline with speed (V), has zero elevation and the system operates in a ground plane (Cherniakov *et al*., 2006; RSA Raja Abdullah *et al*., 2003). Assuming the transmitting signal bandwidth Δf, the bistatic range resolution ΔR_{BR} could be specified by:

$$\Delta R_{BR} = \frac{c}{2\Delta f_t \cos(\beta/2)} \tag{1}$$

Where c is the speed of light, β is the bistatic angle and for the FSR.

$$\Delta R_{br} \rightarrow \infty \ \beta \rightarrow 180^{o}$$

TABLE 1
Example of vehicle types used in experiment

Mercedes E-class - W124	
Proton Savy	
Proton Myvi	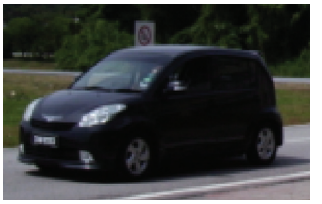

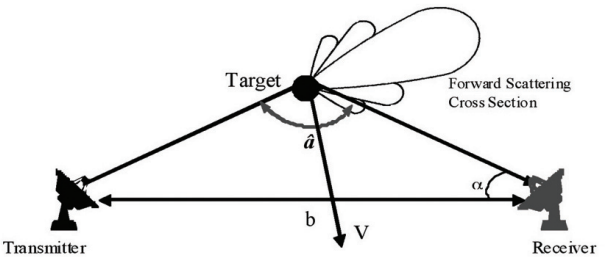

β - bistatic angle

Fig. 1: Forward Scattering Radar general layout (top view), α is the angle on the horizontal plane

As one can see, the transmitting signal bandwidth in the limiting case does not influence the range resolution, and a continuous wave (CW) can effectively be used in the FSR. It is important to mention that in the case of moving targets, the shadow signal experiences Doppler shift, f_{dbr}. This can be evaluated (Willis, 1995) as:

$$f_{dbr} = 2v \frac{1}{\lambda} \cos \delta \cos (\beta/2) \quad (2)$$

The maximal Doppler shift occurs for the target trajectory normal to the baseline $\delta = 0^o$. Even in this case, the absolute value of the f_{dbr} is essentially less than its maximal rate $f_{dmax} = 2v/\lambda$ corresponding to a monostatic radar. For $\beta = 170^o$ to be considered as a boundary of the FS corridor, the absence of a range resolution and low Doppler shift, even for relatively high-speed targets, introduces a big threat for the FSR from the ground clutters. At the time that β approaches 180^o, the target blocks part of the transmitted signal (i.e. the direct signal from the transmitter), leading to a reduction in the received signal power. In this case, the target acts as an aperture antenna with a maximum gain equal to:

$$G = \frac{4\pi A}{\lambda^2} \tag{3}$$

Where $\lambda = c/f_c$ is the signal wavelength, which is assumed to be small as compared to the dimensions of the target, and A is the target shadow silhouette area projection on the transmitter-target line. When $\beta = 180^0$, the level of received signal, comprising of the scattered signal from the target and transmitted signal, reaches its maximum. Similarly, at this condition, the target radar cross section can be characterized by a forward scattering cross-section (FSCS), which is also dependent upon the target shadow silhouette area A (Cherniakov *et al*., 2006).

$$\sigma_b = \frac{4\pi A^2}{\lambda^2} \tag{4}$$

Using practical numbers, it could be shown that the FSCS is essentially bigger than the corresponding monostatic RCS. For a small car (ground target), with a physical area $A \sim 4\text{m}^2$ at frequency 900 MHz, $\sigma_b = 2000\text{m}^2$ could then be expected when a similar target in the monostatic case had about 50m^2 RCS. This and the robustness to stealth targets are considered as one of the main advantages of the FSR. When the bistatic angle decreases, the FSCS follows the appropriate equivalent antenna pattern. The first null in this pattern occurs at the angular distance (Cherniakov *et al*., 2006).

$$\alpha = \lambda / l_{\max} \tag{5}$$

Where, l_{max} is the maximum length of the target. Equation 5 is a good approximation only for the optical region, that is, where $l_{max} > \lambda$. In the resonance region, $l_{max} \sim \lambda$, forward scattering still exists but this equation is not accurate. Using rectangular targets with different lengths as examples, it was theoretically shown and experimentally confirmed that the cross-section of the target $\sigma_b(\varphi)$, $\varphi = \pi = \beta$, approximately followed the appropriate antenna pattern with a rectangular aperture (RSA Raja Abdullah *et al*., 2003). The received forward-scattering signature is a function of the observation angle α (angular distance in terms of Radar Cross Section). When the target crosses the baseline, it has a maximal cross-section, and this region can be used as the parameters to evaluate the target detect ability. Alternatively, if the bistatic angle never reaches 180^o, an appropriate σ_b reduction should be taken into account and the detection via FSCS side lobes can then take place. For example, for a rectangular silhouette, the cross section reduction follows the $\sin^2(\beta/\Delta\beta)/(\beta/\Delta\beta)^2$ function (Cherniakov *et al*., 2006). This means that if the waveforms are processed using the third side lobe of the FSCS, a signal reduction from 22 dB to 23 dB is expected (Cherniakov *et al*., 2006). It is obvious that the forward scattering components of a moving target introduce a Doppler shift. This can be used for moving target selection, as well as for its speed determination. This

information is also used in the FSR for the trajectory reconstruction and classification of target. The Doppler shift depends mainly on the target velocity vector components and the carrier frequency. The general equation which describes the received waveform, that is, the target signature from the moving sample target (rectangular shape) can be found in Cherniakov *et al*. (2006).

EXPERIMENTAL SET UP AND DATA COLLECTION

In this section, the experimental set-up is described and the method used for data collection is presented. Two experimental setups were implemented to collect the FSR signal. The different parameter between the setups are in the transmitter–receiver distance, types of antenna and height of antenna. Details of the experimental setup are presented in the next sub-sections. Typical cars in the public road were used as examples for the target. Table 1 shows the example of the targets used in the experiment.

Experimental Setup: Layout 1

Fig. 2 illustrates the FS sensor block diagram, the system topology and a typical scene during experimentation used for data collection. The transmitter generates a 20 dBm CW signal at an ISM band carrier frequency of 900 MHz with vertical polarization. In the layout, two directional flat antennas, as shown in *Fig. 3*, were used as the transmitting and receiving antennas. At the receiver end, the vehicle signature is detected via non-linear processing, whereby the arriving signal, containing both direct signal and the signal with the Doppler components, is passed through an amplitude detector. The low-pass filter allows only this Doppler component to pass through. This waveform is the vehicle signature which is stored for further processing.

Experimental Setup: Layout 2

In general, the experimentation in Layout 2 is similar to Layout 1, but the differences are:

i. In the second setup, two omni-directional antennas, with lower gain at 2dbi and wider beamwidth as shown in *Fig. 4*, were used. It is desirable for any radar sensor to have a wide coverage area. In this case, employing the Omni-directional antenna enabled the forward scattering network to cover up to 360^{o} angle. This could happen with a specially designed sensor network topology.
ii. The separation distance, between the transmitter and the receiver, was increased up to ~40m. The transmitter–receiver distance in the initial layout was restricted to only ~15m. As the transmitter receiver distance increases, this will reduce the power received at the receiver, and the signal is highly corrupted with noise. To increase the transmitter receiver, the baseline distance is one of the important requirements in a practical radar system.
iii. The antenna was mounted on the pole and was elevated to ~1m from the ground in the first case (*Fig. 3*), whereas the antenna was directly elevated on the ground in the second experimentation, as shown in *Fig. 4*. With this position, the antenna could be covert and was also less cumbersome due to the non-mounting mechanism, hence is easy to deploy and incurs low cost.

The difference between the two experimental set ups is summarized in Table 2. These differences, especially in the experimental Layout 2, make the process of extracting the Doppler frequencies more difficult. The scenario restricts the power density incident onto the target surface, beside the higher noise level and the ground clutter which is added to the received signal. The choice of using carrier frequency at 900 MHz increases the difficulty of extracting the Doppler signals; this is due to the tendency to experience strong interference, especially from the cellular services. An example of the received signal is shown in the next section.

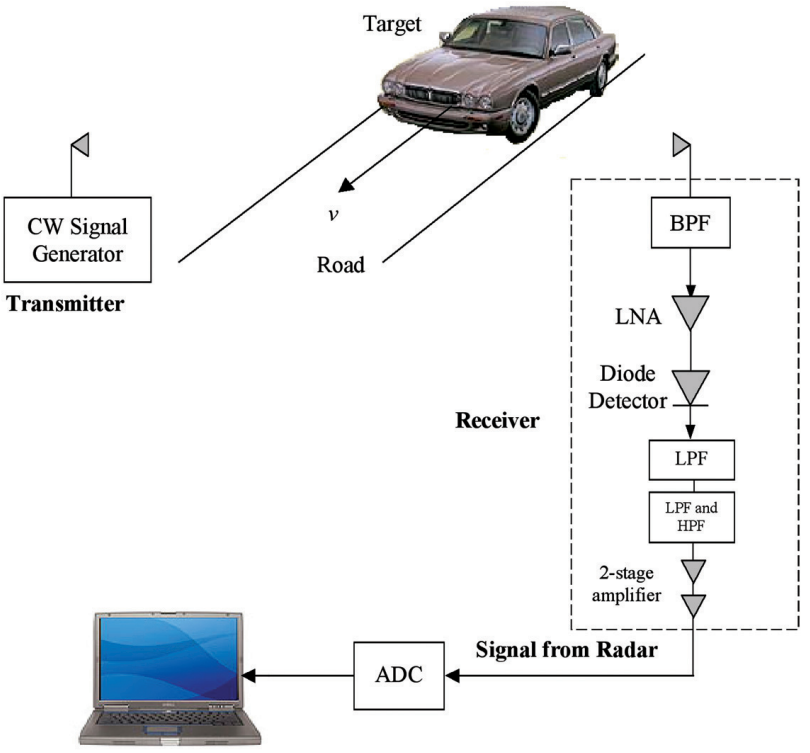
Target
v
Road
CW Signal Generator
Transmitter
BPF
LNA
Diode Detector
Receiver
LPF
LPF and HPF
2-stage amplifier
Signal from Radar
ADC

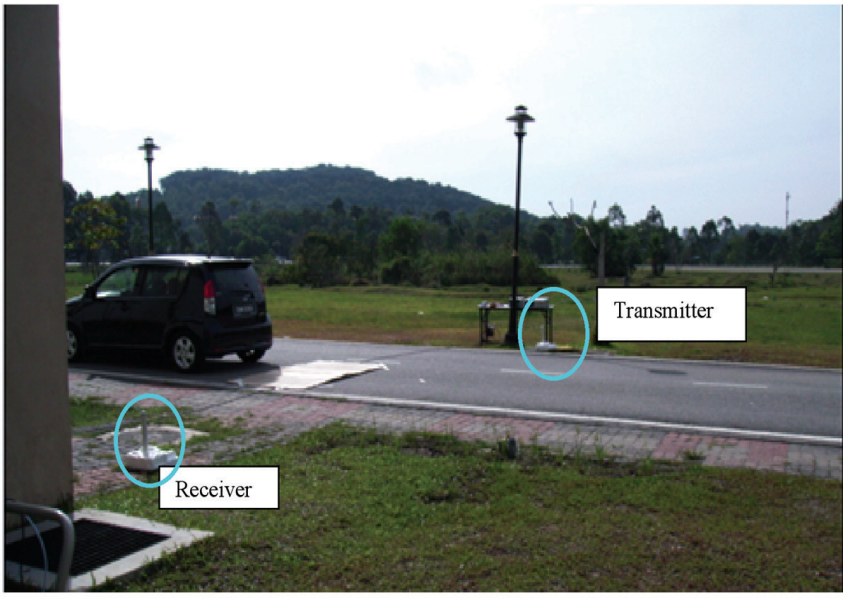
Transmitter
Receiver

(a)

(b)

Fig.2: (a) General experiment layout for the FSR detection, (b) Scene for the FSR target detection experiment

TABLE 2
The difference set up between the two layouts

Factors	Layout 1	Layout 2
Antenna	High gain directional	Low gain omni directional
Tx-Rx separation Distance	Up to 15 m	Up to 40 m
Antenna elevation	Elevated to ~1m from the ground	directly elevated on the ground

TARGET DETECTION IN THE FORWARD SCATTERING RADAR

In the FSR system, as shown in *Fig. 1*, the electromagnetic wave scattered from the target carries Doppler information to the receiver, as a result of the changes in the transmitter-target-receiver distance. The Doppler frequency is determined by the carrier wavelength, λ, while the target's speed relative to the receiver is as given by Equation 2 in Section 2. In the case of the FSR, by looking at Equation 2 and as illustrated in *Fig. 5* (using a point target), the Doppler frequency scattered by the target is zero whenever the target is exactly on the transmitter – receiver baseline (position 'C', f_{Dc}=0). Hence, the first detection technique of the target's existence within the FSR corridor is

Fig. 3: Directional antenna used in Layout 1

Fig. 4: Dipole omni directional antenna

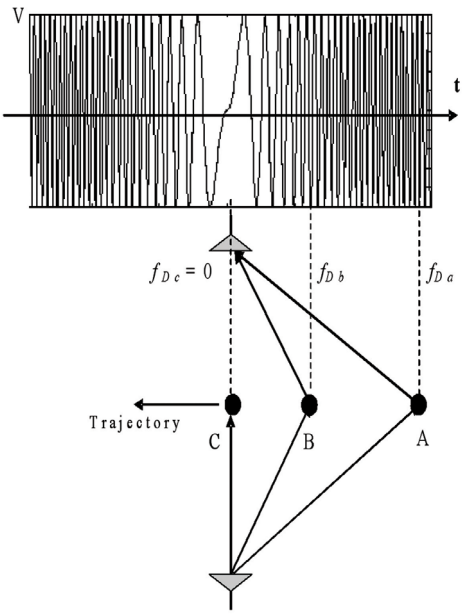

Fig. 5: Doppler frequency variation relative to the scattering point on the vehicle

based on the high amplitude of zero Doppler frequency (DC component) at the receiver, i.e. when the target is exactly on the transmitter–receiver baseline. The Doppler frequency at the receiver increases as the target moves away from the baseline.

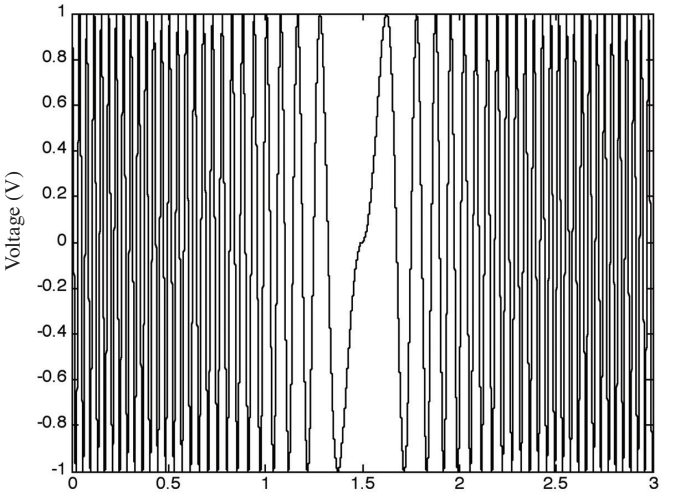

(a)

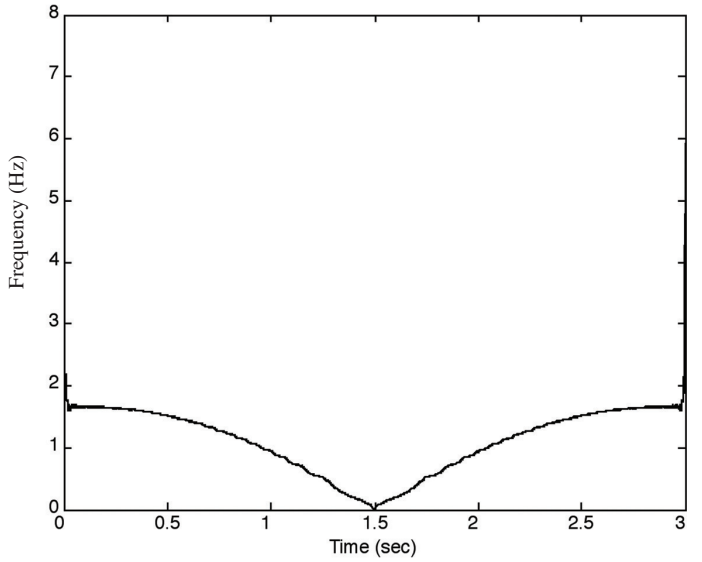

Fig. 6: Ideal analytical signal in (a) time domain and (b) its instantaneous frequency

By employing the Hilbert transform to the received signal, it produces a relationship between the instantaneous frequencies with respect to time, reflecting the position of the target. From the discussion in Section 2 and the assumption given above, zero frequency or very low frequency is created at the time that the object passes through the FSR baseline, and using the frequency–time relationship from Hilbert, the target can then be detected. The effectiveness of the proposed method is presented first by testing to the analytical result, and followed by the real experimental data.

To calculate the instantaneous frequency, f_i the Hilbert Transform of the received signal, x(t) was performed and given by: (Marple, 1999)

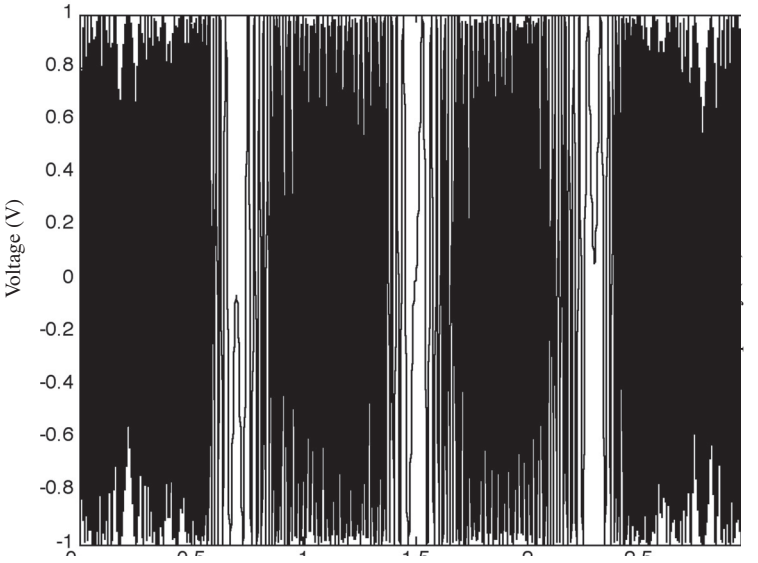

(a)

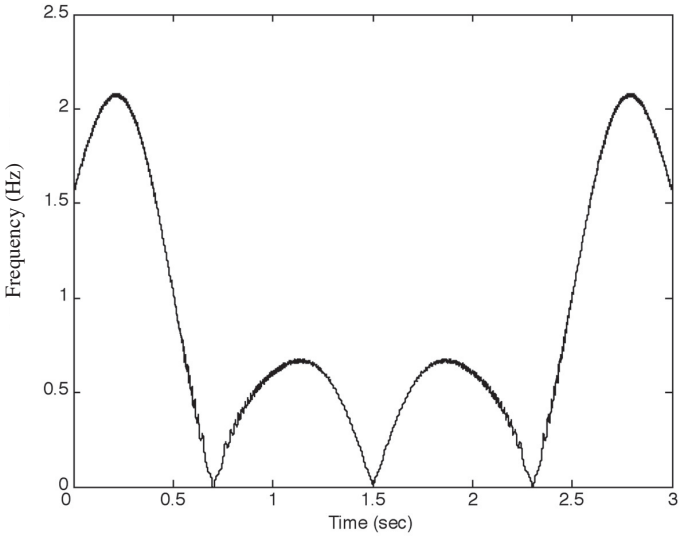

Fig. 7: Analytical signal from the three targets in (a) time domain and (b) its instantaneous frequency

$$z(t) = x(t) + i \times y(t) \tag{6}$$

Where $z(t)$ is the notation for the Hilbert Transform, and $y(t)$ represents the complex conjugate of $x(t)$. In this case, the instantaneous frequency is defined as the rate of phase change of the angle between y(t) and x(t), divided by 2π. *Figs. 6a* and *6b* show n theoretical ideal received Doppler signal, from one target and its frequency-time relationship, respectively. Another example in *Fig.*

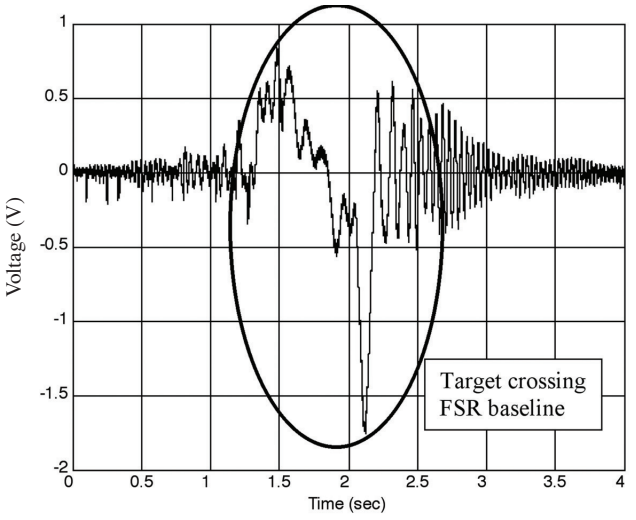

(a)

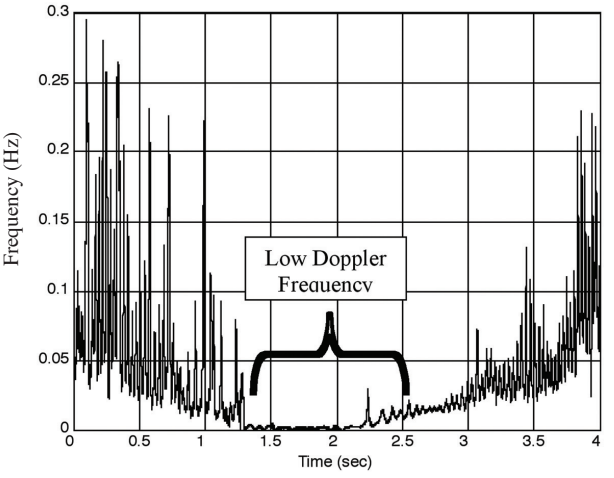

(b)

Fig. 8: Received signal from Layout 1 (a) time domain (b)its instantaneous frequency

7a shows the theoretical received signal from three targets and the frequency-time relationship is presented in *Fig. 7b*. The plots showing the instantaneous frequency-time relationship (*Figs. 6b* and *7b*) clearly show the target crossing the baseline (zero Doppler frequency) correlates with the position in the time domain signal (*Figs. 6a* and *7a*). Thus, this technique can be used for target detection in the FSR.

Next, the frequency–time relationship is produced by performing the Hilbert Transform to the real received signal from the experiment using Layout 1. *Fig. 8a* shows an example of the received signal in time domain from Layout 1. The frequency-time relationship, after the Hilbert Transform, is shown in *Fig. 8b*. Again, from the example, the proposed method and assumption were validated.

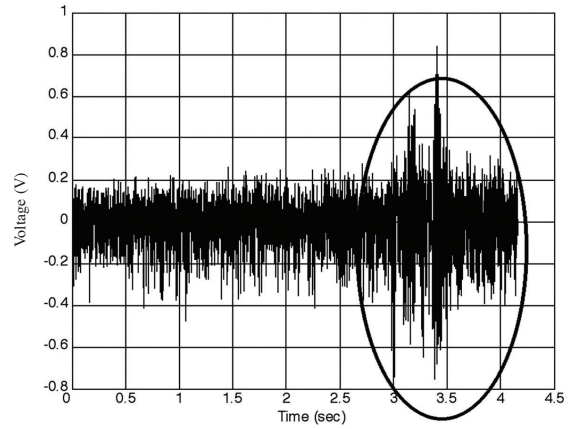

(a)

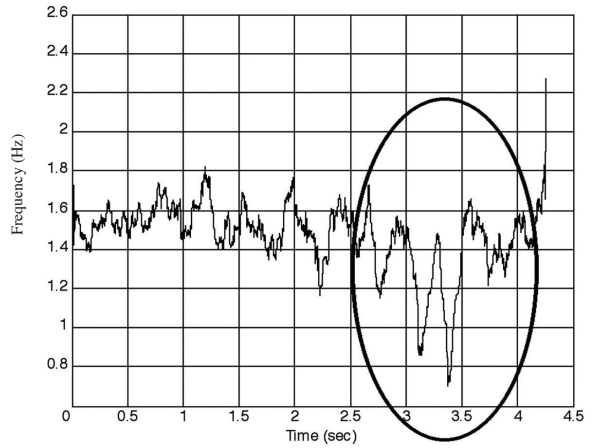

(b)

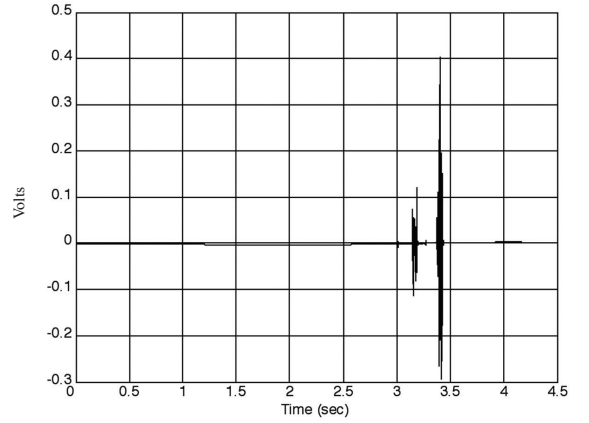

(c)

Fig. 9: Received signal from Layout 2 20m separation distance (a) time domain, b) Its instantaneous frequency, (c) Wavelet denoised received signal

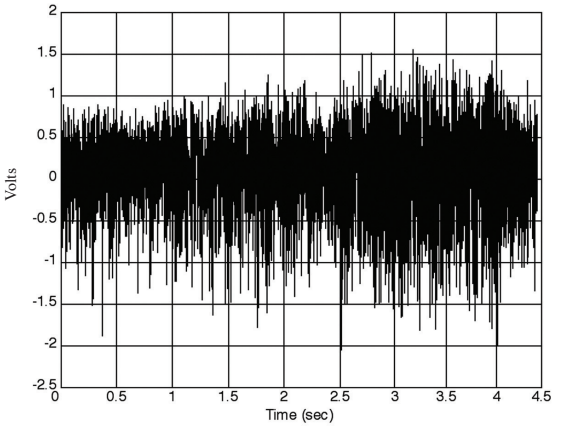

(a)

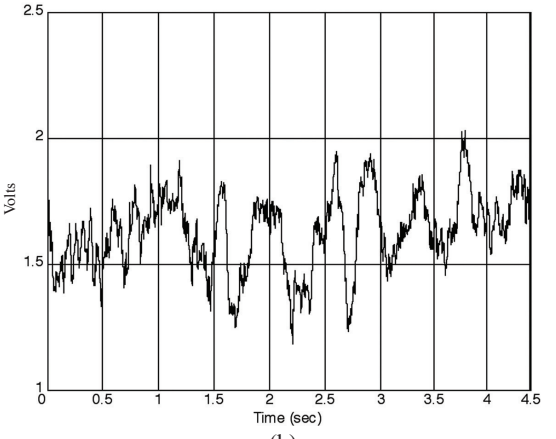

(b)

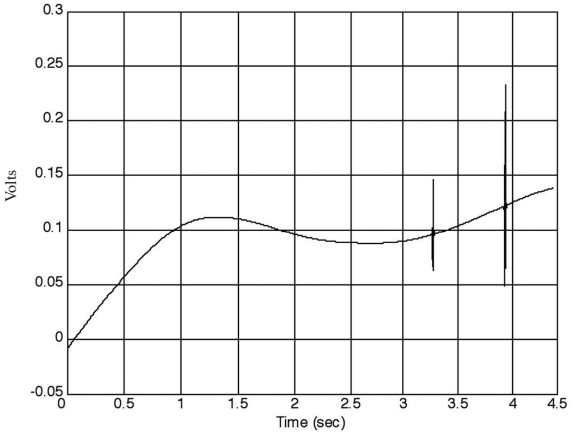

(c)

Fig.10: Received signal from Layout 2 20m separation distance (a) time domain (b) Its instantaneous frequency and (c)Wavelet denoised received signal

Zero and very low Doppler frequency is clearly seen from the trace in the graph of *Fig. 8b*. Thus, the detection of a target is possible and the crossing time can also be predicted.

The instantaneous frequency-time relationship, using the Hilbert Transform to this signal sample, does not give a huge significant contribution. This is due to the huge interruption on the time domain signal (*Fig. 8a*). Nevertheless, this exercise has at least shown a reliable assumption and a possibility to detect the presence of target using the proposed procedure. This is also amongst the first documented result to show the instantaneous frequency-time relationship in the practical FSR system for a better understanding.

The next step is to apply the same procedure to the FSR data, using the experimentation given in Layout 2. In this experiment, the transmitter-receiver distance was increased to ~40m and the antennas were placed directly on the ground. During the experimentation, two targets with a separation distance of approximately ~3m were crossing the baseline at a speed ~20km/h. The two targets were almost similar in shape and they had at least the same maximum height. *Fig. 9a* shows the received signal in time domain. The plot shows that the signals from the targets are under the influence of high noise and can barely be seen by human visualization.

Fig. 9b shows the trace of the instantaneous frequency–time relationship from the Hilbert Transform as in the previous case. This figure reveals a promising indicator, based on the two lowest frequencies, between 3 and 3.5 sec. The positions of these two minimum peaks do correlate with the expected target's signal in time domain. Each low peak represents each car which passes the FSR baseline. The result is considered good, provided the target existence is known beforehand. However, if these plots (*Fig. 9a*) are to be processed by an automatic detection, a few more parameters have to be taken into account, for example, the frequency threshold (acceptable lowest frequency) before any decision can be made, and the minimum difference between the frequency from the target and clutter. These factors will create uncertainties and false alarm in the radar system.

Based on these examples, if the transmitter receiver distance is further increased or transmitting signal power is reduced, or both, the Doppler information will completely be hidden and embedded inside the ground clutter. Thus, it is less efficient if the target existence is predicted using the frequency–time relationship. This relationship is illustrated in *Fig. 10* for the increased transmitter receiver distance, and *Fig. 11* for the reduced transmitted power. An example of these signals will be given in the subsequent section, while an alternative method to detect the existence of target in the FSR system will also be discussed.

DENOISING USING WAVELET

To overcome the uncertainties in decision making, a denoising technique of the received signal using wavelet is proposed. This procedure can increase the confidence in target detection in the FSR system. Lehmann and Teschlke (2001) gave an example of using the wavelet for denoising in a radar system. In this paper, the wavelet denoise was used to automatically remove both ground and intermittent clutters (air plane echoes) from wind profiler radar data.

The signal denoising using wavelet comprises of three steps, namely Decomposition, Threshold Detail Coefficients and Reconstruct. After the signal decomposition using wavelet transform, the signal is left with a set of wavelet coefficients which correlate to the high frequency sub-bands. These high frequency sub-bands consist of the details in the signal. If these details were small enough, they might be omitted without substantially affecting the main features of the signal. However, these small details are often associated with noise; therefore, by setting these coefficients to zero, the noise are essentially filtered out from the signal. This is the idea of thresholding, setting all subs band frequency coefficients which are less than a particular threshold to zero, and using these coefficients in an inverse wavelet transformation to reconstruct the signal.

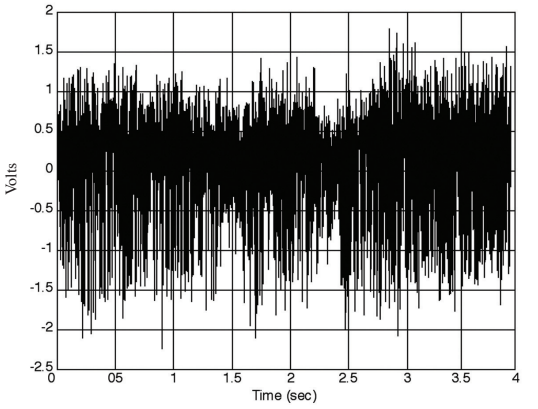

(a)

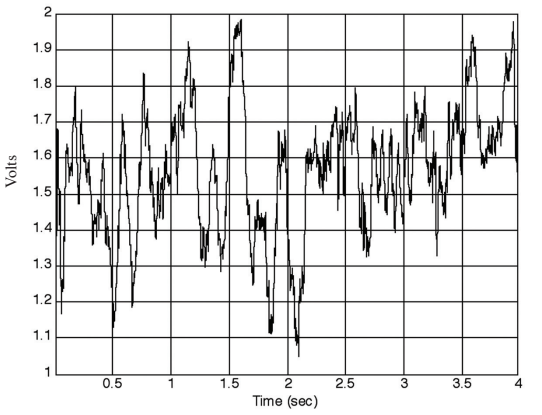

(b)

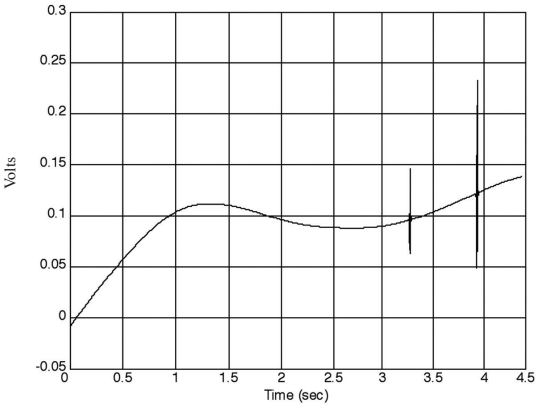

(c)

Fig. 11: Received signal from Layout 2 20m separation distance and reduced transmit power (0 dBm) a) time domain, (b) its instantaneous frequency, (c) Wavelet denoised received signal

The following sub-section explains the mathematical descriptions for the wavelet denoise, and how it is applied in the detection technique in the FSR. Let the first level of decomposition denoted by A_j where *j* is the number of decomposition, and assume $(A_k^j)_k \in z$ as the coordinates of the vector A_j and k could be time in this case.

The initialization is carried out using $A_k^0 = s(k)$, where *s(k)* is the signal value at time *k*. By equating s(t) = s(k), where s(t) is the received signal from target at the receiver, it is given by (RSA Raja Abdullah *et al*., 2003):

$$s(t) = \frac{k\lambda}{2\pi vt(d)} \sin\left(\frac{2\pi}{\lambda}\{\frac{vt}{d}\}\right) e^{-j\frac{4\pi}{\lambda}(d)} \tag{7}$$

Hence, we have

$$A = \sum_k A_k^{(j)} \phi_{j,k} \tag{8}$$

Where $\phi_{j,k}$ scaling function is used to calculate the approximations, and $A_k^{(j+1)}$ is the coordinate of the vector A_{j+1}, then

$$A_{J+1} = \sum_K A_K^{(J+1)} \phi_{J+1,K} \tag{9}$$

Where $A_k^{(j+1)}$ is calculated using the formula

$$A_K^{(J+1)} = \sum h_{n-2k} A_n^{(J)} \tag{10}$$

This formula resembles a convolution formula. Now let us define
$\tilde{h}(k) = h(-k)$, and $F^{(j+1)} = \sum_n \tilde{h}_{k-n} A_n^{(j)}$

The sequence $F^{(j+1)}$ is the filtered output of the sequence A^j by the filter $\tilde{h}$. Hence,

$$A_k{}^{(J+1)} = F_{2k}{}^{(j+1)} \tag{11}$$

We have to take the even index values of *F*, this is down sampling of the version $F^{(j+1)}$. The initialization is carried out using, $A_K{}^{(0)} = s(k)$ where *s(k)*is the signal value at time k. The details will follow the same procedure, but instead of filter *h*, filter *g* will be used. Setting to zero, the values above define the threshold, the final denoised signal will be:

$$s = A_j + \sum_{j \le J} D_J \tag{12}$$

Where D is the 'Detail' of the Decomposition.

By denoising the signal in *Fig. 9a*, the signal is left with two peaks and most of the high frequency noises have been filtered out, as shown in *Fig. 9c*. The position of the two very clear high peaks correlated with *Figs. 9a* and *9b*. This validates the denoising process and is adequate for target detection.

To test the feasibility of both the proposed procedures in target detection, similar experiment using Layout 2 had been conducted with the increased transmitter and receiver distance (*Fig. 10*) and also reduced transmit power (*Fig. 11*). This was done to make sure that the signal scattered from target had completely been masked by the clutter and noise. In this example, the scattered

signal was completely masked by the clutter and it was almost impossible to detect the existence of the target within the coverage area. This makes the detection using frequency-time relationship (*Figs. 10b* and *11b*) and denoising more challenging.

Using the denoising technique on the received signal, it is clear that there are two high peaks which correspond to the two targets, as shown in *Figs. 10c* and *11c*. This proves that the proposed technique has worked and successfully detected the target. All the signals, results and traces for the 'before' and 'after' denoising were verified using a video camera capturing the experimentation scene. During the experimentation, all the vehicles which passed through the sensor baseline were recorded using a video camera. This allowed the researchers to associate a captured vehicle signature with the respective vehicle.

Based on the analysis and the examples, the target detection in the FSR has been shown to be influenced by the level of power and the hardware used. This effect can be seen in the example using a high gain and narrow beam width antenna. In this case, the Doppler signature is clear due to the low noise levels and high SNR. In the second example, the detection process is more difficult when the antenna is replaced by low gain and wide beam width omni directional antenna with the same level of transmit power due to the low SNR. This factor becomes clearer when the transmit power is decreased, and it is impossible to detect the existence of a target directly without using an advanced signal processing to denoise the signal. Thus, signal processing using wavelet technique, which contains high pass and low pass filter coefficients in the example shown in this paper, has successfully denoised the complex signals.

CONCLUSIONS

In this paper, a signal processing and experimental study for extracting the Doppler signature in the FSR for ground target detection have been presented. The target signal under the influence of high clutter has successfully been detected using the proposed method. The detection using the Hilbert Transform is only applicable if the raw signal has significant difference from the average noise level, but detection using the wavelet denoising becomes more robust to any clutter and noise. The results again confirmed the feasibility of the FSR to be employed as an automatic ground target detection system. However, to make the FSR ready to be realized in real applications, more work still needs to be done, including practical cross range resolution in the FSR and an advanced classification technique.

REFERENCES

Abdullah, R., Cherniakov, M. and Jancovic, P. (2004). Automatic vehicle classification in Forward Scattering Radar. In *First International Workshop on Intelligent Transportation WIT* (pp. 7-12). Hamburg, Germany.

Blackman, A.B. and Runova, I.A. (1999). Forward scattering radiolocation, Bistatic RCS and Target Detection. In *Radar Conference*, *1999. The Record of the 1999 IEEE*, pp. 203-208.

Blackman, A.B., Ryndyk, A.G. and Sidorov, S.B. (2000). Forward Scattering Radar moving object coordinate measurement. *Proc. Int.Radar Conf*., pp. 678–682. Washington, DC, USA.

Boyle, R.J. (1994). Comparison of mononstatic and bistatic bearing estimation performance for low RCS targets. *IEEE Transactions on Aerospace and Electronic System, 30*(3), 962-968.

Chapurskiy V.V. and Sablin, V.N. (2000). SISAR: Shadow Inverse Synthetic Aperture Radiolocation. *International Radar Conference*, *The Record of the IEEE 2000 International*, pp. 322 – 328.

Cherniakov, M., Chapurskiy, V.V., Raja Abdullah, R.S.A., Jancovic, P. and Salous, M. (2004). Short-range Forward Scattering Radar, *International Radar Conference*, The Record of the IEEE International, pp. 322 – 328.

Cherniakov, M., Salous, Kostylev and Abdullah, R.S.A. (2005). Analysis of Forward Scattering Radar for ground target detection. *European Radar Conference*, pp.145 – 148.

Cherniakov, M., Abdullah, R.S.A.R., Jancˇovicˇ, P., Salous, M. and Chapursky, V. (2006). Automatic ground target classification using Forward Scattering Radar, *IEE Proc.- Radar Sonar Navig*., *153*(5), 427 – 437.

Chernyak. (1998). *Fundamentals of Multisite Radar Systems*. Gordon and Breach Science Publishers.

Chesnokov, Y.S. and Krutikov, M.V. (1996). Bistatic RCS of aircrafts at the forward scattering. Radar, 1996. *Proceedings, CIE International Conference of Radar*, pp. 156 – 159.

Glaser, J.I. (1985). Bistatic RCS of complex objects near forward scatter. *IEEE Transactions on Aerospace and Electronic System, AES-21*(1), 70-78.

Gould, D.M., Orton, R.S. and Pollard, R.J.E. (2002). Forward Scatter Radar detection. *RADAR 2002*, 15-17, pp. 36 – 40.

Jackson, M.C. (1986). The geometry of bistatic radar systems. *IEE Proceedings, 133*(7), 604-612.

Lehmann, V. and Teschlke, G. (2001). Wavelet based methods for improved wind profiler signal processing. *Annals Geophysical, 19*, 825-836(c). European geophysical society.

Marple, S.L. (1999). Computing the discrete-time analytic signal via FFT. *IEEE Transactions on Signal Processing, 47*(9), 2600-2603.

Raja Abdullah, R.S.A. and Cherniakov, M. (2003). Forward Scattering Radar for vehicles classification. *VehCom International Conference, VehCom2003*, pp. 73-78. Birmingham, UK.

Siegel, K.M. (1985). Bistatic radars and forward scattering. *National Conference Proceeding in Aeronautical Electronics*, pp. 286-290. Ohio.

Stimson, G.W. (1983). Introduction to Airborne Radar. Hughes Aircraft Company, El Segundo, California, pp. 3.

Willis N. J. (1995). Bistatic Radar. Technology Service Corporation.